An Impedance Matching Method for LC Passive Wireless Sensors

Ming-Zhu Xie, Li-Feng Wang, *Member, IEEE*, Bin-Bin Zhou, and Qing-An Huang, *Fellow, IEEE*

***Abstract*—This paper presents an impedance matching method for increasing the readout distance of an inductor-capacitor (LC) passive wireless sensor. When the impedance of the LC sensor system is equal to that of the measurement system, there is no reflection between the LC sensor system and the measurement system, which maximizes signal-to-noise ratio and readout distance. Complex impedance matching networks at the readout port of the LC sensor system have been analyzed and simulated. The matching capacitor at the readout port is required to change with the sensing capacitor in the LC sensor in order to maintain the same resonant frequency in both readout port and LC sensor. The matching resistor at the readout port has been analyzed and optimized. A varactor-based capacitor was inserted as the matching capacitor, which can be controlled by a DC voltage so that the resonant frequency of the readout port can be scanned within the full range of resonant frequency in the LC sensor. A capacitive humidity sensor constructed from a planar spiral inductor and an interdigital capacitor was used here to demonstrate the proposed impedance matching method. It shows that the readout distance under the impedance matching is 1.5 times as long as that without the impedance matching. The impedance matching analysis gives in-depth insight into the LC sensor system behavior, and the results presented here suggest that the impedance matching method may be utilized the long distance readout of the scaled LC sensor application based on the S_{11} measurement.**

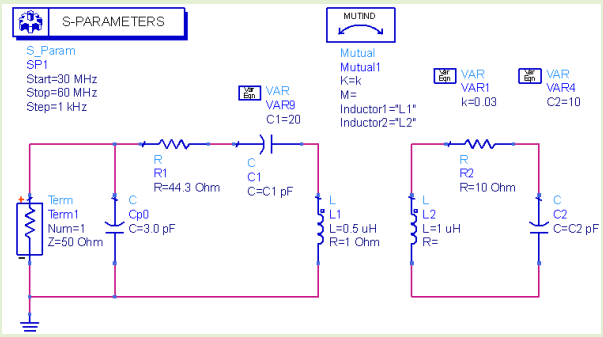

***Index Terms*—Passive wireless sensor, readout enhancement, impedance matching.**

I. Introduction

INDUCTOR-CAPACITOR (LC) passive wireless sensors consist of a capacitive sensing element in resonance with a coil that is inductively coupled with an external readout coil, as shown in Fig.1 (a) [1], [2]. Because of their simple, batteryless, and wireless capabilities, they have been utilized in a number of applications such as medical and industrial areas [3]. In particular, microelectromechanical systems (MEMS) technology scaling helps to reduce the size of the LC sensor, which makes it possible to monitor intraocular pressure or intravascular blood pressure via implantable devices [3]–[13], wound pressure via wearable devices [14], [15], humidity in micropackages [16], [17]. However, the coupling strength decreases as the size of the coils decreases, so a small coil in the LC sensor results in a very low coupling factor, which inevitably leads to a short readout distance.

Many efforts have been made to extend the readout distance of LC passive wireless sensors. A ferrite core can dramatically increase the inductance when compared with an air core. Harpster *et al.* added a ferrite core in the central of the sensor inductor, which confines magnetic field to realize a stronger coupling between the readout coil and the sensor coil, and hence achieving a longer readout distance [16]. However, the appearance of the ferrite will enlarge the equivalent resistance of the inductor, causing the Q factor to decrease [18]. Increasing the inductor size can effectively enhance the magnetic coupling between the readout coil and the sensor coil, which extends the readout distance. However, this method has to increase the sensor chip size. Zhang *et al.* achieved a large inductance by using a dual-layer inductor while keeping the same sensor chip size [19]. For the same signal intensity in measurement, the readout distance of the *LC* sensor with the higher Q factor is longer than its counterpart with the lower Q factor. Based on a new figure of merit, Yeon *et al.* optimized geometries for both the sensing and inductive link components of the LC sensor, leading to the longer readout distance [13]. Adding an additional resonant repeater between the readout coil and the sensor coil would enhance the magnetic coupling over a longer distance. This scheme has been used in wireless

Manuscript received March 17, 2020; revised June 10, 2020; accepted June 18, 2020. Date of publication June 22, 2020; date of current version October 16, 2020. This work was supported in part by the National Key Research and Development Program of China under Grant 2018YFB2002500 and in part by the National Natural Science Foundation of China under Grant 61136006, Grant 61401084, and Grant 61801110. The associate editor coordinating the review of this article and approving it for publication was Dr. Thilo Sauter. *(Corresponding author: Qing-An Huang.)*

The authors are with the Key Laboratory of MEMS of the Ministry of Education, Southeast University, Nanjing 210096, China (e-mail: hqa@seu.edu.cn).

Digital Object Identifier 10.1109/JSEN.2020.3004146

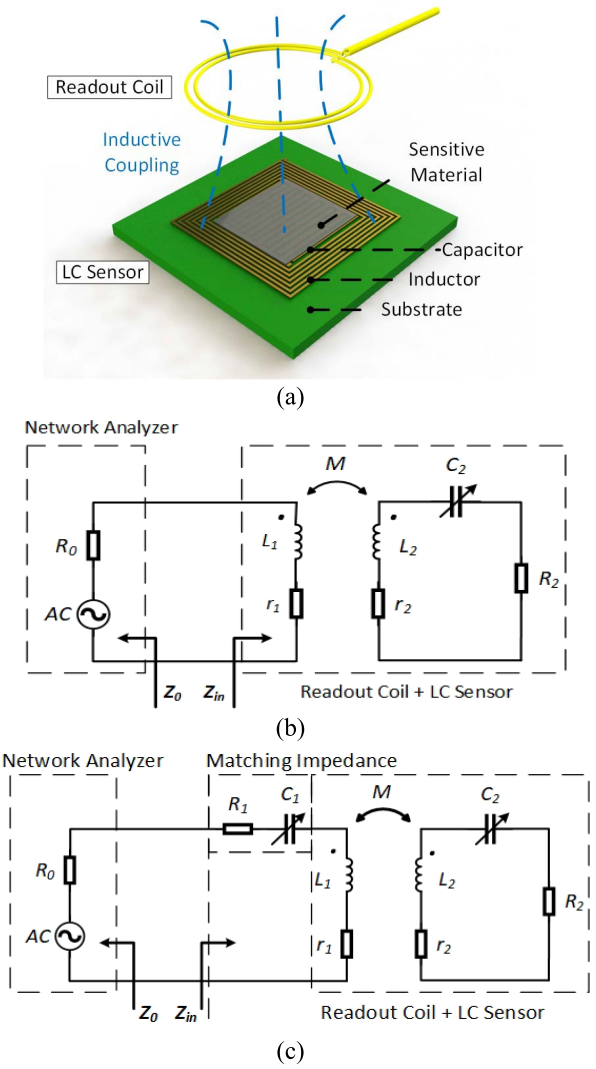

Fig. 1. (a) Schematic of an LC passive wireless sensor and readout system. (b) The equivalent circuit for a non-matching inductively coupled LC passive wireless sensor system. (c) The equivalent circuit for an impedance matching inductively coupled LC passive wireless sensor system.

power transfer for midrange applications [20]. When used in LC passive wireless sensor detection, the repeater also operates in passive manner and can enhance the readout [21]–[24]. The above methods have been demonstrated to be able to extend the readout distance of the LC passive wireless sensors with a small footprint to some extent.

On the other hand, there is no area constraint on the readout port, so various kinds of readout approaches have been proposed. Coosemans *et al.* designed a fully differential tuned voltage controlled oscillator (VCO) to excite the LC sensor so as to maximize the sensitivity of the system [25]. Marioli *et al.* considered the leakage and coupled magnetic fluxes, which compensates the change of distance between the readout and LC sensor [26]. Jacquemod *et al.* presented an anti-resonance cancellation architecture in the readout port [27]. Nopper *et al.* introduced an analog frontend circuit based on coherent demodulation for mapping the real part of the readout coil impedance to a dc output voltage [2]. Peterson *et al.* presented a wireless sensor interrogator design based on frequency modulation spectroscopy (FMS), which is capable of wireless detection and tracking of the resonant frequency [28]. Zhang *et al.* presented a portable interrogator by using a standing wave ratio bridge to measure the real part of the readout coil impedance [29]. Wang *et al.* treated the impedance of the readout coil and sensor coupling system as the load for a RF amplifier, leading to a wide frequency measurement range [30]. Schormans *et al.* proposed a miniaturized wireless measurement system by using a self-oscillator and a frequency counter [31]. Overall, these approaches have improved the sensitivity, frequency range, or readout distance of the LC passive wireless sensors. Different from these approaches, this paper has presented an impedance matching method for increasing the readout distance. When the impedance of the LC sensor system is equal to that of the measurement system, there is no reflection between the LC sensor and the measurement system, which maximizes signal-to-noise ratio (SNR) and readout distance. In fact, the impedance matching method has been demonstrated in wireless power transfer (WPT) to improve the power transfer efficiency [32] and in radio frequency identification devices (RFID) to enhance the readout range [33] both at a fixed frequency. When it is applied to the LC passive wireless sensors, the resonant frequency at the readout port of the sensor system has to follow the resonant frequency change of the LC sensor resulting from the changes in the parameter of interest. Hence, the specific matching design for the LC sensor system is needed. In Section II, the impedance matching networks at the readout port of the sensor system have been analyzed and simulated. In Section III, the varactor-based capacitor circuit for impedance matching was introduced, and an LC wireless capacitive humidity sensor was fabricated, measured, and compared with our analysis. Finally, some conclusions and discussions are given in Section IV.

II. Design and Analysis

A. Equivalent Circuit

An LC wireless sensor is generally consist of a spiral inductor connected with a sensing capacitor, forming a LC resonant tank. As shown in Fig.1 (a), to wirelessly interrogate the LC sensor, a readout coil is magnetically coupled with the sensor, and the resonant frequency of the LC sensor is detected through monitoring the impedance or input reflection coefficient of the readout coil. Such telemetric sensor systems are generally modelled as the equivalent circuit shown in Fig.1 (b), where L_1 and L_2 are the self-inductance of the readout coil and the sensor coil, r_1 and r_2 are the parasitic resistance of the readout coil and the sensor coil, R_2 and C_2 are the resistance and capacitance of the LC sensor, respectively. And, M is the mutual inductance, $k = \mathrm{M}/\sqrt{L_1 L_2}$ is the coupling coefficient between the readout coil and the sensor coil. The resonant frequency f_2 and the quality factor Q_2 of the sensor are defined as

$$f_2 = \frac{1}{2\pi\sqrt{L_2 C_2}} \tag{1a}$$

$$Q_2 = \frac{1}{r_2 + R_2}\sqrt{\frac{L_2}{C_2}} \tag{1b}$$

Z_0 and $Z_{in,1}$ are the impedances looking into the measurement system and the readout coil, respectively. They are written as

$$Z_0 = R_0|_{R_0=50\Omega}, \tag{2}$$

$$Z_{in,1} = r_1 + j\omega L_1 + \frac{\omega^2 M^2}{r_2 + R_2 + j\omega L_2 + \frac{1}{j\omega C_2}}, \tag{3}$$

$$Re\left(Z_{in,1}\right) = r_1 + \frac{(2\pi f)^2 M^2}{(r_2+R_2)\left(1+Q_2^2\left(\frac{f}{f_2}-\frac{f_2}{f}\right)^2\right)}, \tag{4}$$

$$Im\left(Z_{in,1}\right) = 2\pi f L_1 - \frac{(2\pi f)^2 M^2 Q_2\left(\frac{f}{f_2}-\frac{f_2}{f}\right)}{(r_2+R_2)\left(1+Q_2^2\left(\frac{f}{f_2}-\frac{f_2}{f}\right)^2\right)}. \tag{5}$$

where Z_0 is the characteristic impedance of the measurement system, which is usually equal to 50Ω for the Vector Network Analyzer. $Re\left(Z_{in,1}\right)$ and $Im\left(Z_{in,1}\right)$ are the real part and the imaginary part of $Z_{in,1}$.

B. Impedance Matching

The reflection coefficient at the terminals of the readout port (Fig.1 b), S_{11}, as a function of the measured impedance Z_{in} with respect to the measurement system characteristic impedance Z_0 is written as

$$S_{11} = \left.\frac{Z_{in} - Z_0}{Z_{in} + Z_0}\right|_{Z_0=50\Omega}, \tag{6a}$$

$$S_{11}\,(dB) = 20log\,|S_{11}|\,. \tag{6b}$$

Generally, in a readout system without impedance matching, the magnitude of S_{11} will get its minimum near the resonant frequency of the LC sensor [15], [34]. Furthermore, if the impedance of the readout port Z_{in} is exactly equal to the measurement system characteristic impedance Z_0, S_{11} parameter will be zero, which means there is no reflection between the sensor system and the measurement system. Since Z_0 is a real number and Z_{in} is a complex number, it yields

$$Re\,(Z_{in}) = R_0 \tag{7a}$$

$$Im\,(Z_{in}) = 0. \tag{7b}$$

According to equations (4) and (5), the readout impedance is a function of frequency f, only at the resonant frequency of the sensor f_2, the input impedance satisfies the impedance matching condition can maintain the information of the sensor. However, f_2 changes in response to parameters of interest, equation (7) cannot be met all the time. The impedance matching circuit is put forward here, as shown in Fig.1(c), where a series resistor R_1 and a series capacitance C_1 are added in the readout port. Then, the readout impedance $Z_{in,2}$ of the impedance matching LC sensor system is now written as

$$Z_{in,2} = r_1 + R_1 + j\omega L_1 + \frac{1}{j\omega C_1} + \frac{\omega^2 M^2}{r_2 + R_2 + j\omega L_2 + \frac{1}{j\omega C_2}}, \tag{8}$$

$$Re\left(Z_{in,2}\right) = r_1 + R_1 + \frac{(2\pi f)^2 M^2}{(r_2 + R_2)\left(1 + Q_2^2\left(\frac{f}{f_2} - \frac{f_2}{f}\right)^2\right)}, \tag{9}$$

$$Im\left(Z_{in,2}\right) = Q_1\,(r_1 + R_1)\left(\frac{f}{f_1} - \frac{f_1}{f}\right) - \frac{(2\pi f)^2 M^2 Q_2\left(\frac{f}{f_2} - \frac{f_2}{f}\right)}{(r_2 + R_2)\left(1 + Q_2^2\left(\frac{f}{f_2} - \frac{f_2}{f}\right)^2\right)} \tag{10}$$

where

$$f_1 = \frac{1}{2\pi\sqrt{L_1 C_1}}, \tag{11a}$$

$$Q_1 = \frac{1}{r_1 + R_1}\sqrt{\frac{L_1}{C_1}}. \tag{11b}$$

Inserting equations (9) and (10) into (7), the optimum parameters for the readout circuits are given by

$$C_{1m} = \frac{L_2 C_2}{L_1}, \tag{12}$$

$$R_{1m} = R_0 - \frac{k^2 L_1}{C_2\,(r_2 + R_2)} - r_1. \tag{13}$$

In order to achieve optimum impedance matching at f_2, equations (12) and (13) need to be satisfied at the same time. C_{1m} corresponds to the resonance condition that the readout port and LC sensor must have the same resonant frequency. R_{1m} is the optimum resistance matching condition. When the coupling coefficient or the quality factor of the LC sensor is very large, the optimum matching resistance will become negative. However, in most cases of the LC sensor, the quality factor is low due to skin effects, eddy currents and surrounding environment, and the coupling coefficient is small for a long range readout. Therefore, the optimum resistance is usually positive. The matching resistance R_1 can adjust the impedance matching degree and control the readout intensity. As shown in Fig.2 (a), if the matching resistance R_1 is less than the optimum matching resistance R_{1m}, the signal magnitude $|S_{11}|$ at resonant frequency f_2 will reduce, but its minimum occurs at resonant frequency f_2. If the matching resistance is larger than the optimum resistance R_{1m}, the signal magnitude $|S_{11}|$ will also reduce at first, then there is a splitting frequency as shown in Fig.2 (b). To avoid the frequency splitting, the matching resistance had better equal to or less than the optimum value.

C. Simulation Results

To compare the overall performance of LC passive wireless sensors with and without the impedance matching, the simulations were conducted in the advanced design system (ADS). Since R_1 and r_1 are in series, R_2 and r_2 are in series, $R_1 + r_1$ and $R_2 + r_2$ will be replaced by R_1 and R_2 in simulation, respectively. The parameters used in the simulations are listed in Table I.

Firstly, the simulation of an LC passive wireless system without impedance matching was conducted. The circuit

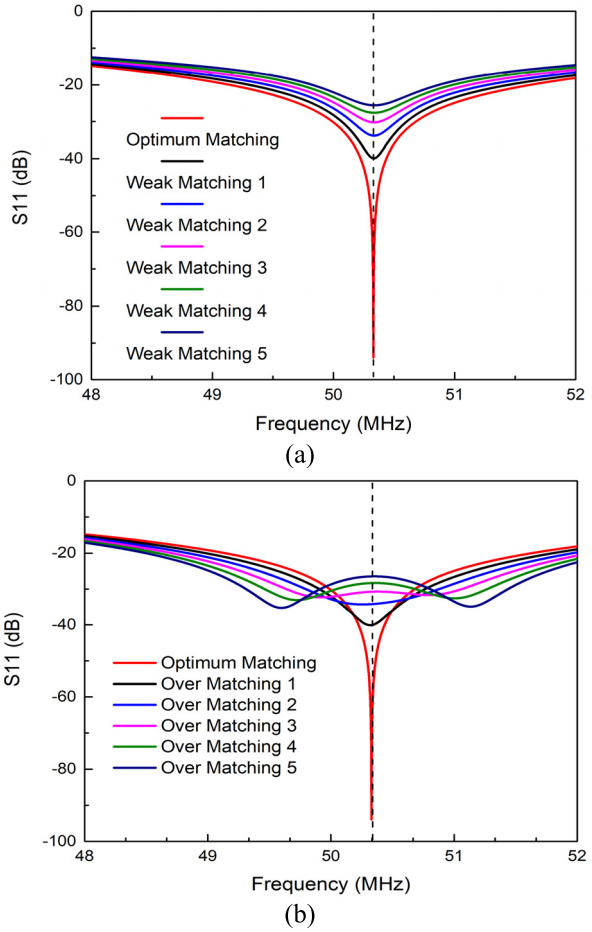

Fig. 2. The effect of different resistors on the impedance matching. (a) The magnitude of S_{11}(dB) versus frequency for different weak matching resistances. (b) The magnitude of S_{11} (dB) versus frequency for different over matching resistances.

TABLE I
CIRCUIT PARAMETERS IN ADS SIMULATION

Symbol	L_1	L_2	R_2	C_2
Value	0.5μH	1μH	10Ω	10pF~20pF

schematic is shown in the inset of Fig. 3(a). The coupling coefficient k between the readout coil and the sensor coil is 0.03. When the sensor capacitor C_2 increased from 10pF to 20pF with a step of 2pF, the resonant frequency of the sensor f_2 is shown in the minimum S_{11}, which monotonously decreased from 50.35MHz to 35.60MHz. The signals magnitude detected by the readout coil without impedance matching at k = 0.03 are less than 0.15dB, as presented in Fig. 3(a).

Secondly, the matching capacitor C_1 and resistor R_1 were added into the readout port with k = 0.03. A sweep was conducted in C_1 to find the matching optimum capacitor, which satisfies the resonant condition, $L_1C_1 = L_2C_2$. Once the resonance happens, a strong signal can be detected. Assuming the sensor capacitance C_2 is fixed at 18 pF and the matching resistance R_1 is the optimum matching value, simulation results are obtained in Fig. 3(b). Each curve in Fig. 3(b) has two valleys corresponding to the resonant frequency f_1 of the readout tank and the resonant frequency f_2 of the LC sensor. Owing to the small coupling coefficient here, the reflected

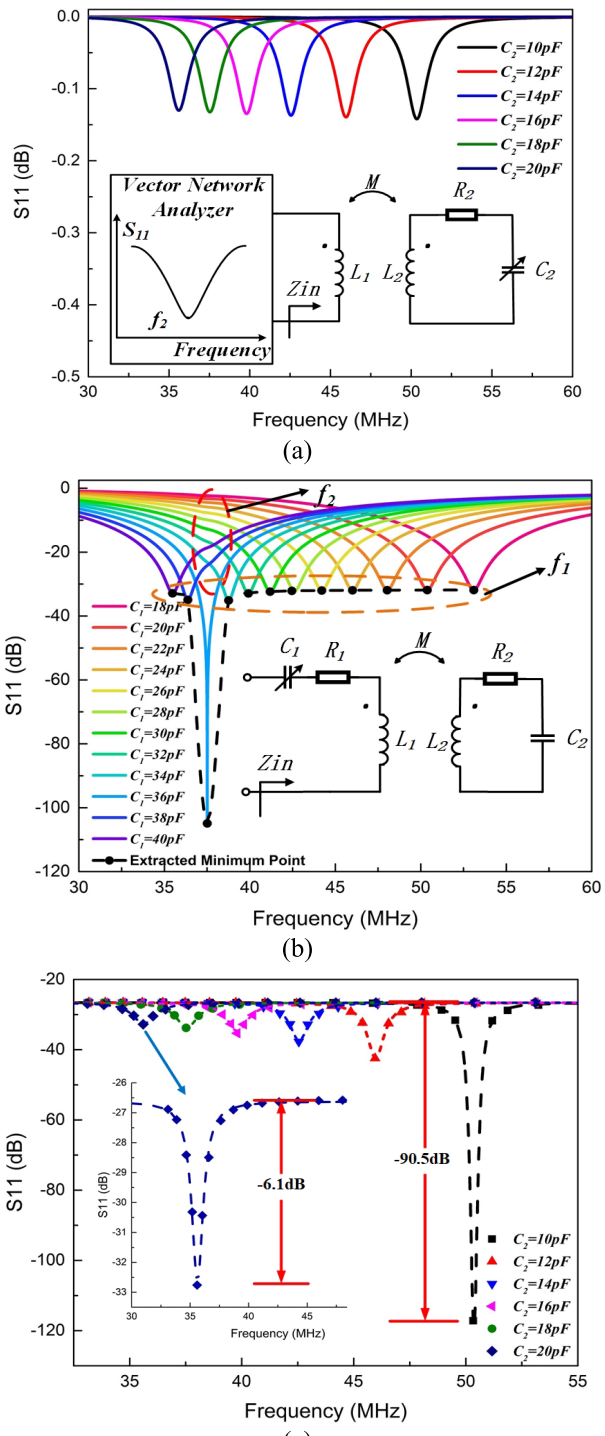

Fig. 3. ADS simulation results. (a) The magnitude of S_{11} (dB) versus frequency detected by the conventional readout port. (b) Scanning line for different capacitances of C_1. There is a sharp reflection dip at 37.51MHz, which is the common resonant frequency of the readout port and sensor. (c) Extracted resonant frequency points at different capacitances of C_2.

signal intensity at f_2 is small compared with the signal of the readout tank, so the valley at f_2 is not obvious. When f_1 is far away from f_2, the signal intensity is almost the same, which is a baseline of the effective signal. When f_1 comes close to f_2, the readout S_{11} signal begins to decrease, and when f_1 is consistent with f_2, the S_{11} signal shows up

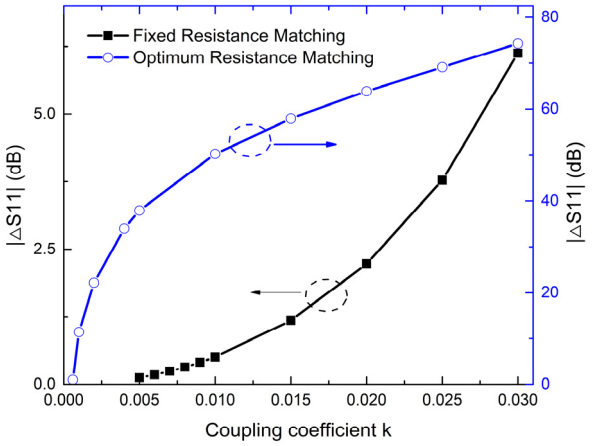

Fig. 4. The effective signal intensity $|\Delta S_{11}|(dB)$ versus coupling coefficient using the fixed and optimum matching resistance at the readout port.

a sharp dip. The signal intensity difference ΔS_{11} between the amplitude of the minimum valley value (sensor signal) and the baseline (readout tank signal) is the effective signal intensity, which determines the recognizable sensor signal. If all the corresponding minimum points of each line are extracted, and then the fitting curve of the resonant points is given in the dark dash line in Fig. 3(b). It shows that the effective signal difference is -72.95dB, which is much stronger than the LC sensor without impedance matching.

Another matching condition is the matching resistance R_1, which affects the signal intensity. According to equation (13), the optimum matching resistance is dependent of the coupling coefficient, the sensing capacitance and other components, which is hard to implement in a practical circuit readout system. Fortunately, when the matching resistance is less than the optimum value, the readout signal also can be enhanced, as explained in Section B. Then, R_1 is set to be 45.5Ω, which is the optimum matching resistance at $C_2 = 10pF$.

The final simulation result detected by the impedance matching system is shown in Fig.3 (c), the coupling coefficient is kept at 0.03. It can be seen that all the signal intensities are obviously enhanced even R_1 is fixed, among which the minimum signal enhancement is -6.1dB at $C_2 = 20pF$, showing that it is 30 times more than the signal intensity detected by the non-matching readout at the same coupling coefficient. Hence, the readout signal intensity is enhanced by the proper fixed matching resistor at the readout port.

The effective signal intensity $|\Delta S_{11}|$(at $C_2 = 20pF$) as a function of coupling coefficient using different matching resistances was also simulated by ADS. The results are shown in Fig.4. The minimum detectable coupling coefficient using the optimum matching resistance is 0.0006 while it is 0.005 using the fixed matching resistance. Both fixed and optimum matching resistance at the readout port can extend the minimum detectable coupling coefficient, which validates the readout distance can be extended by the fixed matching resistance.

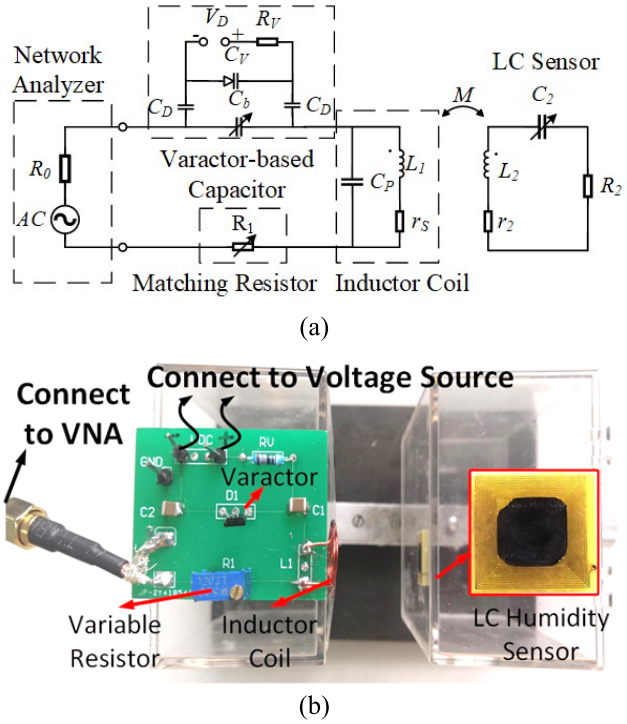

Fig. 5. (a) Schematic of designed matching circuit. (b) The measurement system with the impedance matching. The left is the designed matching circuit, and the right is the LC passive wireless humidity sensor.

III. Experiments and Discussions

To experimentally verify our proposed scheme, an impedance matching circuit was developed, a LC humidity sensor was used to measure, and compared with the result without the impedance matching circuit.

A. LC Humidity Sensor

The humidity sensor consists of a planar spiral inductor and an interdigital capacitor made on print circuit board (PCB), as shown in the inset of Fig. 5 (b). The line width and line spacing of the interdigital capacitor are both $100\mu m$.The line length of the interdigital capacitor is 0.5cm, and the number of the interdigital pair is 14. The outer diameter and the inner diameter of the inductor are 1cm and 0.65cm, respectively. The number of the turns of the inductor is 12. The inductance of the inductor was tested to be $2.55\mu H$. The graphene oxide was dropped on the interdigital capacitor as the moisture sensing material, and the sensor was baked in dying oven at 50° for 2 hours. And the measured resonant frequency of the humidity sensor was 54.26MHz at 15% RH and 25°C, corresponding to $C_2 = 3.73pF$.

B. Impedance Matching Circuit

To apply impedance matching to the readout port, a variable resistor and a varactor-based capacitor are added. The prototype of the matching system was implemented and the equivalent circuit diagram is shown in Fig. 5. C_V(BB910, 2∼20pF) is the voltage dependent junction capacitor. C_D

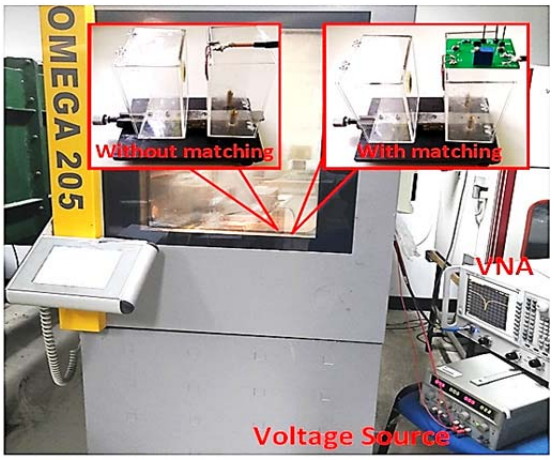

Fig. 6. Experiment setup of the readout system with and without the impedance matching.

(10μF) is the decoupling capacitor to reduce noise from DC voltage source coupled to the detector power supply. C_b is the frequency-selection capacitor used to select frequency spectrum to cover the sensor frequency. R_V (1 MΩ) is used to block the RF signal from the DC voltage source. The varactor-based capacitor was controlled by a DC voltage source, so that the resonant frequency of the readout coil can be scanned within a frequency spectrum which covers the full range of the LC sensor operating resonant frequency. R_1 is the variable resistor. L_1, R_s, and C_p are the series inductance, resistance and the parasitic parallel capacitance of the readout inductor coil, respectively. The readout coil is made by copper wire with 3.5-turn and a diameter of 1.5 cm. The frequency response of the LC sensor was detected by vector network analyzer (VNA) through the S_{11} minimum.

C. Experiment Setup and Measurement Results

To compare the signal intensity and the readout distance between the readout circuit with and without impedance matching, the same inductor coil was used as the readout antenna. The experiment setup is shown in Fig. 6. The LC sensor and the readout circuit were attached to two moveable holders of the displacement platform, respectively. The readout equipment is PNA Network Analyzer (N5224A, Agilent Technologies). A DC voltage source (Model MPS-3003L-3) is used to change the varactor-based capacitor. The readout circuit without the impedance matching only has an inductor coil. The humidity test was done in the OMEGA 205 chamber. The relative humidity was raised from 15%RH to 90%RH with a step of 15%RH, while the temperature was kept at 25 °. The same minimum signal intensity to noise ratio (SNR) is taken as the criterion of the performance enhancement, the signal is the effective signal intensity $|\Delta S_{11}|$, and the noise is the jitter signal difference caused by the environment noise.

The LC humidity sensor was firstly detected by the non-matching circuit. The distance between the sensor and the readout coil was 1.5cm. Fig. 6 (a) gives the detected S_{11} parameter versus frequency. The resonant frequency decreases from 54.26MHz to 49.47MHz. The measured sensitivity of the humidity sensor is about −63.86 kHz/%RH. The S_{11} intensity and the Q-factor decrease with the increased relative humidity. The minimum signal intensity $|\Delta S_{11}|$ (dB) is 0.04dB at 90%RH, the signal noise is 0.01dB, and the SNR is 4. Therefore, the maximum readout distance of the inductor readout system without impedance matching is 1.5cm.

Secondly, the readout circuit with the impedance matching was detected. According to the impedance matching theory proposed in Section II, it is essential to find a proper fixed matching resistance prior to tests. First, the distance between the sensor and readout coil was fixed at 1.5cm, and the humidity test chamber was set to 15%RH. The capacitance was then scanned to search the matching resonant frequency point, according to the appearance of a valley minimum. The variable resistance was adjusted so that the equivalent resistance of the whole LC system was equal to 50Ω at the matching resonant frequency, which can be seen from the Smith chart of the vector network analyzer (VNA). The value of the matching resistance at 1.5cm distance was tested to be 45.2Ω for 25° and 15%RH. So, the matching resistance was fixed at 45.2Ω. The DC voltage was swept manually from 1V to 4V with a step of 0.05V, which can sweep the resonant frequency of the readout port from 45 MHz to 60 MHz with a step of 250 kHz. The scanning lines at a part of DC voltages are shown as the inset of Fig. 7(b). The minimum points of the S_{11} scanning lines were extracted and recorded to form the effective response signal. The sharp dip in the extracted signal corresponds to the resonant frequency of LC sensor.

The whole response of the humidity sensor detected by the impedance matching circuit at different relative humidity levels is shown in Fig.7 (b). The resistance of 45.2Ω is the optimum matching for 15%RH, hence the signal intensity at 15%RH is the largest. 90%RH is the most mismatched case, hence the signal intensity is the smallest. It can been seen that the Q-factor decreases with the increased relative humidity. The resonant frequency decreases from 54.19MHz to 49.82MHz. The measured sensitivity of the humidity sensor is about −58.26 kHz/%RH. The difference from the non-matching results is caused by the low DC voltage source step and the instability of the humidity chamber. The sharp dip in S_{11} parameter suggests that the impedance matching readout circuit leads to larger signal intensity enhancement.

In order to verify the readout distance enhancement, the matching resistance was kept at 45.2Ω, and the readout distance of the matching readout system was adjusted to make its SNR be equal to that of the non-matching readout system. The signal enhancing performance with the impedance matching can be intuitively reflected to the readout distance. The obtained distance was 2.25cm, which is 1.5 times as long as the distance of the non-matching readout system. When the distance is extended, the detected signal intensity will decrease, and will be influenced by the oblique baseline signal, which is caused by the parasitic parallel capacitor in the readout port. The influence can be eliminated by subtracting the baseline signal. The whole humidity response after subtracting the baseline signal is shown in Fig. 7(c), the humidity response is similar to the result detected by the non-matching readout coil at 1.5cm, the S_{11} intensity and the Q-factor decrease with the increased relative humidity. The signal intensity at 90%RH

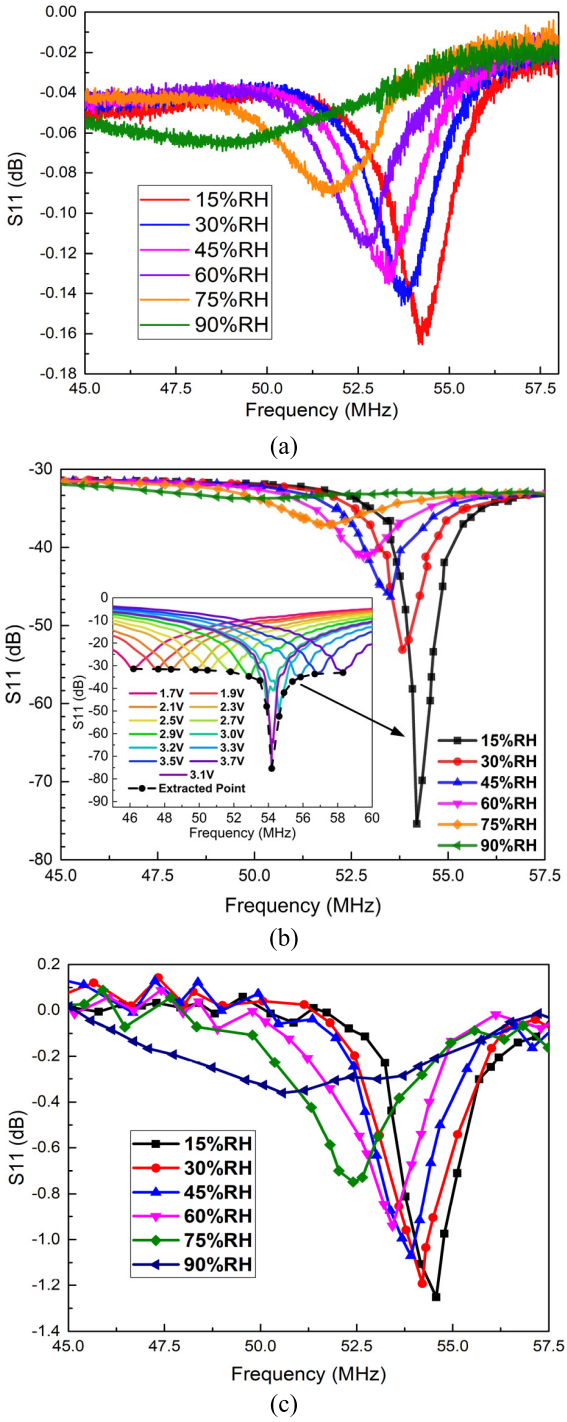

Fig. 7. (a) The humidity response detected by the non-matching readout circuit at a distance of 1.5cm. (b) The humidity response detected by the matching readout circuit at a distance of 1.5cm. The inset is the scanning line at different DC voltages. (c) The humidity response detected by the matching readout circuit at a distance of 2.25cm.

is 0.4dB, the noise intensity is 0.1dB, and the SNR is 4, which is the same as the non-matching readout at 90%RH.

The resonant frequency as a function of humidity level detected by the two different readout systems is shown in Fig.8. The resonant frequency response trends are the same among different readouts. For the impedance matching readout system, the resonant frequency detected at 2.25cm is larger than the resonant frequency detected at 1.5cm, and the relative

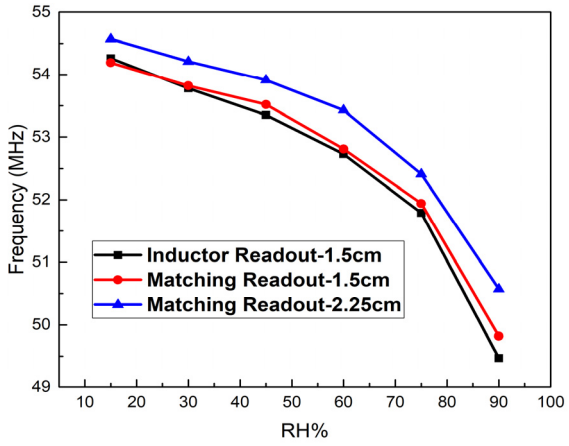

Fig. 8. The resonant frequency of the LC humidity sensor as a function of relative humidity, detected by the two different readout ports.

error between them is less than 1.2%. The difference between the matching and non-matching results is caused by the low DC voltage source step and the instability of the humidity chamber. The resonant frequency deviation between different distances is caused by the parasitic parallel capacitance in the readout port [35]. More precious readout circuit can be realized by adding a circuit topology to compensate the readout parasitic capacitance [36].

D. Measurement Time and Measurement Resolution

The measurement time is the execute time to change the DC voltage plus the stable time to get the right frequency response plus the PNA frequency sweep time plus the data store time, then multiply the DC voltage sweep numbers. The time for PNA Network Analyzer (N5224A, Agilent Technologies) to sweep from 45 MHz to 60 MHz with a step of 10 kHz is 10.897ms. We use the manual process to change the DC voltage and store the data, so we need about 3s to execute the voltage change, wait for the signal to stable and record one S_{11} minimum signal. The voltage was swept from 1V to 4V with a step of 0.05V, which can cover the resonant frequency of the readout circuit from 45 MHz to 60 MHz with a step of 250 kHz. The sweep number is 61. So, the total measurement time is 3 min for manual process, this method can be optimized using the microcontroller to speed up the process to few seconds.

The measurement resolution is depend on the frequency sweep step and the voltage sweep step. The smaller the sweep step, the higher the resolution, but the more measurement time. The measurement resolution in this paper is 250 kHz restricted by the low DC voltage source step.

IV. Conclusions

In summary, the impedance matching approach at the readout port for LC passive wireless sensor system is proposed and demonstrated. The closed-form formulations for the matching conditions are given, and a circuit design has been performed. A scanning capacitance circuit has been designed to search the optimum matching capacitance so that the matching capacitance condition can be satisfied. A matching resistance is simulated and discussed, and a fixed matching resistance is adopted here. Both the ADS simulation and the experiment

results show the impedance matching readout design can enhance the readout signal intensity or increase the readout distance. The LC humidity sensors have been utilized to verify the readout distance enhancement. It shows that the readout distance under the impedance matching is 1.5 times as long as that without the impedance matching. The impedance matching method proposed here may be utilized in the long distance readout of the other scaled LC sensor.

REFERENCES

[1] C. C. Collins, "Miniature passive pressure transensor for implanting in the eye," *IEEE Trans. Biomed. Eng.*, vol. BME-14, no. 2, pp. 74–83, Apr. 1967.

[2] R. Nopper, R. Has, and L. Reindl, "A wireless sensor readout system–circuit concept, simulation, and accuracy," *IEEE Trans. Instrum. Meas.*, vol. 60, no. 8, pp. 2976–2983, Aug. 2011.

[3] Q.-A. Huang, L. Dong, and L.-F. Wang, "LC passive wireless sensors toward a wireless sensing platform: Status, prospects, and challenges," *J. Microelectromech. Syst.*, vol. 25, no. 5, pp. 822–841, Oct. 2016.

[4] L. Rosengren, Y. Backlund, T. Sjostrom, B. Hok, and B. Svedbergh, "A system for wireless intra-ocular pressure measurements using a silicon micromachined sensor," *J. Micromech. Microeng.*, vol. 2, no. 3, pp. 202–204, Sep. 1992.

[5] S. Lizón-Martínez, R. Giannetti, J. L. Rodríguez-Marrero, and B. Tellini, "Design of a system for continuous intraocular pressure monitoring," *IEEE Trans. Instrum. Meas.*, vol. 54, no. 4, pp. 1534–1540, Aug. 2005.

[6] K. Takahata, Y. B. Gianchandani, and K. D. Wise, "Micromachined antenna stents and cuffs for monitoring intraluminal pressure and flow," *J. Microelectromech. Syst.*, vol. 15, no. 5, pp. 1289–1298, Oct. 2006.

[7] P. Cong, W. H. Ko, and D. J. Young, "Wireless batteryless implantable blood pressure monitoring microsystem for small laboratory animals," *IEEE Sensors J.*, vol. 10, no. 2, pp. 243–254, Feb. 2010.

[8] P.-J. Chen, S. Saati, R. Varma, M. S. Humayun, and Y.-C. Tai, "Wireless intraocular pressure sensing using microfabricated minimally invasive flexible-coiled LC sensor implant," *J. Microelectromech. Syst.*, vol. 19, no. 4, pp. 721–734, Aug. 2010.

[9] N. Xue, S.-P. Chang, and J.-B. Lee, "A SU-8-based microfabricated implantable inductively coupled passive RF wireless intraocular pressure sensor," *J. Microelectromech. Syst.*, vol. 21, no. 6, pp. 1338–1346, Dec. 2012.

[10] G. Chitnis, T. Maleki, B. Samuels, L. B. Cantor, and B. Ziaie, "A minimally invasive implantable wireless pressure sensor for continuous IOP monitoring," *IEEE Trans. Biomed. Eng.*, vol. 60, no. 1, pp. 250–256, Jan. 2013.

[11] L. Y. Chen *et al.*, "Continuous wireless pressure monitoring and mapping with ultra-small passive sensors for health monitoring and critical care," *Nature Commun.*, vol. 5, no. 1, Art. no. 5028, Oct. 2014.

[12] M. G. Allen, "Micromachined endovascularly-implantable wireless aneurysm pressure sensors: From concept to clinic," in *Proc. 27th IEEE Int. Conf. Micro Electro Mech. Syst. (MEMS)*, San Francisco, CA, USA, Jan. 2014, pp. 1–4.

[13] P. Yeon, M.-G. Kim, O. Brand, and M. Ghovanloo, "Optimal design of passive resonating wireless sensors for wearable and implantable devices," *IEEE Sensors J.*, vol. 19, no. 17, pp. 7460–7470, Sep. 2019.

[14] J. Kim *et al.*, "Wearable smart sensor systems integrated on soft contact lenses for wireless ocular diagnostics," *Nature Commun.*, vol. 8, no. 1, Apr. 2017.

[15] W.-J. Deng, L.-F. Wang, L. Dong, and Q.-A. Huang, "LC wireless sensitive pressure sensors with microstructured PDMS dielectric layers for wound monitoring," *IEEE Sensors J.*, vol. 18, no. 12, pp. 4886–4892, Jun. 2018.

[16] T. J. Harpster, S. Hauvespre, M. R. Dokmeci, and K. Najafi, "A passive humidity monitoring system for *in situ* remote wireless testing of micropackages," *J. Microelectromech. Syst.*, vol. 11, no. 1, pp. 61–67, 2002.

[17] Q.-Y. Ren, L.-F. Wang, J.-Q. Huang, C. Zhang, and Q.-A. Huang, "Simultaneous remote sensing of temperature and humidity by LC-type passive wireless sensors," *J. Microelectromech. Syst.*, vol. 24, no. 4, pp. 1117–1123, Aug. 2015.

[18] M. Saidani and M. A. M. Gijs, "Three-dimensional miniaturized power inductors realized in a batch-type hybrid technology," *J. Micromech. Microeng.*, vol. 12, no. 4, pp. 470–474, Jul. 2002.

[19] C. Zhang, L.-F. Wang, Q.-A. Huang, L. Guo, and J.-Q. Huang, "Passive wireless integrated humidity sensor based on dual-layer spiral inductors," *Electron. Lett.*, vol. 50, no. 18, pp. 1287–1289, Aug. 2014.

[20] A. Kurs, A. Karalis, R. Moffatt, J. D. Joannopoulos, P. Fisher, and M. Soljacic, "Wireless power transfer via strongly coupled magnetic resonances," *Science*, vol. 317, no. 5834, pp. 83–86, Jul. 2007.

[21] C. Zhang, L. F. Wang, and Q. A. Huang, "Extending the remote distance of LC passive wireless sensors via strongly coupled magnetic resonances," *J. Micromech. Microeng.*, vol. 24, no. 12, pp. 125021-1–125021-9, Dec. 2014.

[22] L. Dong, L.-F. Wang, C. Zhang, and Q.-A. Huang, "A cyclic scanning repeater for enhancing the remote distance of LC passive wireless sensors," *IEEE Trans. Circuits Syst. I, Reg. Papers*, vol. 63, no. 9, pp. 1426–1433, Sep. 2016.

[23] L. Dong, L.-F. Wang, and Q.-A. Huang, "A passive wireless adaptive repeater for enhancing the readout of LC passive wireless sensors," *IEEE Microw. Wireless Compon. Lett.*, vol. 26, no. 7, pp. 543–545, Jul. 2016.

[24] L. Dong, L.-F. Wang, and Q.-A. Huang, "Applying metamaterial-based repeater in LC passive wireless sensors to enhance readout," *IEEE Sensors J.*, vol. 18, no. 4, pp. 1755–1760, Feb. 2018.

[25] J. Coosemans, M. Catrysse, and R. Puers, "A readout circuit for an intra-ocular pressure sensor," *Sens. Actuators A, Phys.*, vol. 110, nos. 1–3, pp. 432–438, Feb. 2004.

[26] D. Marioli, E. Sardini, M. Serpelloni, and A. Taroni, "A new measurement method for capacitance transducers in a distance compensated telemetric sensor system," *Meas. Sci. Technol.*, vol. 16, no. 8, pp. 1593–1599, Aug. 2005.

[27] G. Jacquemod, M. Nowak, E. Colinet, N. Delorme, and F. Conseil, "Novel architecture and algorithm for remote interrogation of battery-free sensors," *Sens. Actuators A, Phys.*, vol. 160, nos. 1–2, pp. 125–131, May 2010.

[28] B. J. Peterson, A. V. Olson, and T. J. Kaiser, "A wireless sensor interrogator design for passive resonant frequency sensors using frequency modulation spectroscopy," *IEEE Sensors J.*, vol. 10, no. 12, pp. 1884–1890, Dec. 2010.

[29] C. Zhang, L.-F. Wang, J.-Q. Huang, and Q.-A. Huang, "An LC-type passive wireless humidity sensor system with portable telemetry unit," *J. Microelectromech. Syst.*, vol. 24, no. 3, pp. 575–581, Jun. 2015.

[30] F. Wang, X. Zhang, M. Shokoueinejad, B. J. Iskandar, J. E. Medow, and J. G. Webster, "A novel intracranial pressure readout circuit for passive wireless LC sensor," *IEEE Trans. Biomed. Circuits Syst.*, vol. 11, no. 5, pp. 1123–1132, Oct. 2017.

[31] M. Schormans, V. Valente, and A. Demosthenous, "A low-power, wireless, capacitive sensing frontend based on a self-oscillating inductive link," *IEEE Trans. Circuits Syst. I, Reg. Papers*, vol. 65, no. 9, pp. 2645–2656, Sep. 2018.

[32] N. Inagaki, "Theory of image impedance matching for inductively coupled power transfer systems," *IEEE Trans. Microw. Theory Techn.*, vol. 62, no. 4, pp. 901–908, Apr. 2014.

[33] J. J. Baek, S. W. Kim, K. H. Park, M. J. Jeong, and Y. T. Kim, "Design and performance evaluation of 13.56-MHz passive RFID for E-skin sensor application," *IEEE Microw. Wireless Compon. Lett.*, vol. 28, no. 12, pp. 1074–1076, Dec. 2018.

[34] H. Y. Lee, B. Choi, S. Kim, S. J. Kim, W. J. Bae, and S. W. Kim, "Sensitivity-enhanced *LC* pressure sensor for wireless bladder pressure monitoring," *IEEE Sensors J.*, vol. 16, no. 12, pp. 4715–4724, Jun. 2016.

[35] M.-Z. Xie, L.-F. Wang, L. Dong, W.-J. Deng, and Q.-A. Huang, "Low cost paper-based LC wireless humidity sensors and distance-insensitive readout system," *IEEE Sensors J.*, vol. 19, no. 12, pp. 4717–4725, Jun. 2019.

[36] M. Demori, M. Baù, M. Ferrari, and V. Ferrari, "Electronic technique and circuit topology for accurate distance-independent contactless readout of passive LC sensors," *AEU-Int. J. Electron. Commun.*, vol. 92, pp. 82–85, Aug. 2018.

Ming-Zhu Xie received the B.S. degree in electronic engineering from Southeast University, Nanjing, China, in 2013. She is currently pursuing the Ph.D. degree with the Key Laboratory of MEMS of the Ministry of Education, Southeast University.

Her current research interests include MEMS sensors and passive wireless sensors.

Li-Feng Wang (Member, IEEE) received the B.S., M.S., and Ph.D. degrees in electrical engineering from Southeast University, Nanjing, China, in 2003, 2006, and 2013, respectively. From 2006 to 2008, he was with the Nanjing Electronic Device Institute, where he worked on silicon micromechanical devices.

After graduation, he joined the Faculty of the Department of Electronic Engineering, Southeast University, as an Assistant Professor, where he became an Associate Professor in 2017. His current research interests include the design, fabrication and reliability of wireless micro-sensors and micromachined RF/MW switches.

Bin-Bin Zhou received the B.S. degree in physics from Hebei University, Baoding, China, in 2014, and the M.S. degree in particle physics and nuclear physics from Beihang University, Beijing, China, in 2017. She is currently pursuing the Ph.D. degree with the Key Laboratory of MEMS of the Ministry of Education, Southeast University.

Her research interests include wireless passive microsensors, inductive telemetry techniques, and the application of PT-symmetry in sensor.

Qing-An Huang (Fellow, IEEE) received the B.S. degree from the Hefei University of Technology, Hefei, China, in 1983, the M.S. degree from Xidian University, Xi'an, China, in 1987, and the Ph.D. degree from Southeast University, Nanjing, China, in 1991, all in electronics engineering.

His Ph.D. research was focused on micromachined GaAs piezoelectric sensors. After graduation, he joined as a Faculty Member with the Department of Electronic Engineering, Southeast University, where he became a Full Professor in 1996, and was appointed as the Chang-Jiang Scholar by the Ministry of Education in 2004. He was the Founding Director of the Key Laboratory of MEMS of the Ministry of Education, Southeast University from 2001 to 2019. He has authored a book *Silicon Micromachining Technology* (Science Press, 1996), edited a book *Micro Electro Mechanical Systems* (Springer, 2018), authored or coauthored four international book chapters and over 200 peer-reviewed international journals/conference papers, and holds over 120 Chinese patents.

Dr. Huang is an Editorial Board Member of the *Journal of Micromechanics and Microengineering*. He was a recipient of the National Outstanding Youth Science Foundation Award of China in 2003. He was the Conference Co-Chair of the SPIE Microfabrication and Micromachining Process Technology and Devices (Proceedings of SPIE), the TPC Co-Chair of the Sixth Asia–Pacific Conference of Transducers and Micro/Nano Technologies (APCOT), Nanjing, in 2012, and a TPC Member of Transducers from 2009 to 2019 and the IEEE Sensors Conference from 2002 to 2016. He has been serving as the Editor-in-Chief of the *Chinese Journal of Sensors and Actuators* since 2005.